International Journal of Mathematical Modeling and Applied Computing
Vol. 1, No. 6, September 2013, PP: 26-40
Available online at http://acascipub.com/Journals.php

Research article

Modeling and Simulation of Myxobacteria Swarming Behavior

Melisa Hendrata

Department of Mathematics, California State University, Los Angeles
5151 State University Drive, Los Angeles, CA 90032, USA.

Phone: (323) 343-2150

E-mail: mhendra@calstatela.edu

Abstract

We present a cell-based model to simulate the swarming behavior of various mutants of myxobacteria. Computational complexity is often known to be one of the biggest obstacles in simulating such biological system as there are too many interacting individuals involved in the system. We derive the scaling law for our model, which together with the concept of superindividuals, enable us to perform large scale simulations that produce identical dynamics as the actual biological colony. This idea can be applied in modeling of systems that involve a high number of autonomous agents. The global swarming patterns for different mutants of myxobacteria produced by our simulations show good phenotypic agreement with those observed in experiments. We further quantify these global patterns by computing the order parameter and show the important role of social motility in cell alignment during swarming. **Copyright © acascipub.com, all rights reserved.**

Keywords: cell-based model, myxobacteria, swarming, global pattern, order parameter.

Introduction

Organized movement of cells is an important factor in a variety of biological processes. Organogenesis and morphogenesis in multicellular organisms require organized migration and passing of signals between cells (Igoshin, Kaiser, Oster, 2004). Unicellular organisms exhibit different swarming patterns and the formation of a macro colony as a result of highly organized cell movement. Biofilm formations in medical devices and host-colonization by pathogens also require coordinated movement of cells. Myxobacteria (*Myxococcus xanthus*) are unicellular prokaryotes that are frequently chosen as a prime model to study bacterial colonization process. They are genetically simple, yet they exhibit spontaneous ordering and complex multicellular interaction that emerge from local interactions between neighboring cells.

Individual myxobacteria cells are rod-shaped with average dimension of 0.5 μm by 3-5 μm. Cell motility plays a crucial role during myxobacteria life cycle as it facilitates cell interactions. Their gliding movement is powered by two types of motility motors, namely the A(adventurous)-motility and the S(social)-motility. The A-motility is associated by extracellular polysaccharide (EPS) slime secretion from several hundred pores at the rear pole of the cell (Wolgemuth et al, 2002). This EPS slime secretion generates the thrust that pushes the cell forward and leaves a trail of slime behind it. When a cell encounters a slime trail previously deposited by other cells on the surface, it tends to turn to an acute angle to follow the trail (Burchard, 1982). The S-motility is driven by retraction of type IV pili at the frontal pole of the cell. When a cell is close enough to other cell or a group of cells, the pili can attach to the fibrils that covers the surface of neighboring cells, and then retract to pull the piliated cell forward (Hodgkin, Kaiser, 1979). A wildtype (A+S+) cell possesses both A and S-motility engines. The A+S- mutant has only the A-motility, while the A-S+ mutant has only the S-motility. These three strains exist and can be studied in a laboratory environment (Kaiser, Crosby, 1983). In addition to these motility engines, it was also found that myxobacteria reverses its gliding directions approximately every 6-8 minutes (Blackhart, Zusman, 1985). During this polarity reversal, the motility engines are switched from pole to pole, which means that pili pulling and slime pushing on their current pole are switched off and become active on the opposite poles (Kaiser, 2003; Kaiser, Yu, 2005).

Social phenotype is known to be the most distinct feature in myxobacteria as individual cell behavior changes while in groups and during its complex life cycle. The life cycle of myxobacteria consists of two main stages, namely the swarming stage and the stage of fruiting body development. The swarming stage is associated with the condition in which there are plenty of nutrient. During this stage, myxobacteria glide on surface and grow as swarms that spread radially away from the center of a colony to gain access to nutrients and oxygen. Swarming reduces competition between cells for nutrients. The swarm consists of thousands of cells which predominantly move as coordinated wolf packs to feed on other bacteria (Kaiser, 2003; Pelling et al, 2006). This pattern of movement directs cells to the edge of the colony. The phase transition from the swarming to the fruiting body development stage occurs when nutrients are depleted. During the developmental stage, the cells no longer grow as individuals, but instead they locally align with one another and merge into streams, which then join to form initial aggregation centers. Cells in early aggregation centers are motile and large spiral patterns are formed. Small adjacent aggregation centers fuse to form larger mounds. When more cells are absorbed into the mounds, they rise up and increase in size and eventually form round multicellular structures, called the fruiting bodies. The cells inside the fruiting bodies differentiate into metabolically resistant myxospores. These myxospores will germinate and become vegetative again when nutrients become available (Kaiser, 2003).

Both continuous and discrete models have been developed previously to model myxobacteria characteristics and their collective behavior at different stages (Alber, Kiskowski, Jiang, 2004; Gallegos, Mazzag, Mogilner, 2006; Holmes, Kalvala, Whitworth, 2010; Kiskowski, Jiang Alber, 2004, Sozinova et al, 2005, 2006; Wu et al, 2006). Hendrata and Birnir (2010) introduced a novel cell-based model that utilizes the concept of Dynamic Energy Budget (DEB) to regulate the phase transition between different stages of the life cycle. Later on, Hendrata et al (2011) identified the minimal elements required for social behavior in myxobacteria by using only the experimentally-determined parameter values in their model, thus removing inaccuracy and artificiality that exist in the previous computational models. In this paper, we present our cell-based model and derive the associated scaling laws, which together with the concept of superindividual, allow us to simulate tens of thousands of cells, thus overcoming high computational cost due to complexity of the model. We simulate the swarming of different mutants of myxobacteria and the global swarming patterns produced show good agreement with those obtained in laboratory experiments. We further compute the order parameter to quantify the contribution of A and S-motility to the degree of cell alignment and organization during swarming.

International Journal of Mathematical Modeling and Applied Computing
Vol. 1, No. 6, September 2013, PP: 26-40
Available online at http://acascipub.com/Journals.php

Materials and Method

Mathematical Model

Our cell-based model is essentially a two-dimensional off-lattice model in which a cell is represented by a string of N nodes. We take $3 \leq N \leq 5$ as the actual cell length varies between 3-5 μm. Cell width is set to be 0.1 of its length. Any consecutive pair of nodes are connected by a segment of length L, as depicted in Figure 1. The cell orientation is defined to be the direction pointing from the lagging pole to the leading pole and it is given by

$$\boldsymbol{C}_k = \frac{\boldsymbol{n}_k^1 - \boldsymbol{n}_k^N}{\|\boldsymbol{n}_k^1 - \boldsymbol{n}_k^N\|}, \tag{1}$$

where $\boldsymbol{n}_k^1$ and $\boldsymbol{n}_k^N$ are the positions of the leading and lagging poles of cell k, respectively.

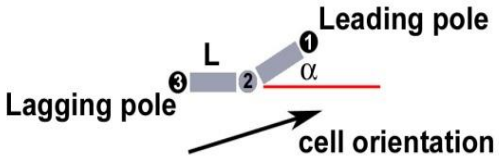

Figure 1: A cell representation with three nodes (N=3) and the vector indicating its orientation. Each segment has a fixed length L and the cell is allowed to turn or bend to an angle α.

In this model we assume that cell movement is driven by the leading pole, which determines the next direction that the cell will move to. Another assumption is that a cell moves with a fixed step length that is set equal to a segment length L. In each iteration, cell k updates its position according to the discrete equation

$$\boldsymbol{x}_k(t + \Delta t) = \boldsymbol{x}_k(t) + v\, \boldsymbol{V}_k(t)\, \Delta t, \tag{2}$$

where $\boldsymbol{x}_k(t)$ denotes the position of the leading pole of cell k at time t, v is cell velocity, Δt is the time step, and $\boldsymbol{V}_k(t)$ is the motility direction at time t. The rest of the nodes will move forward following the leading pole, e.g. node 2 at the next time step $t + \Delta t$ will occupy the position of node 1 at current time t, etc. The direction vector $\boldsymbol{V}_k(t)$ is determined by several factors: cellular reversal, A-motility, S-motility, and collision between cells. We now discuss the algorithm for each mechanism.

Cell reversal

When a cell reverses, the initial leading pole becomes the lagging pole, and vice versa. We assign to each cell a reversal clock and a random reversal period $\boldsymbol{T}_r$ that is normally distributed with mean 6.24 minutes (Shi et al, 2000). Initially, each clock is set to a random phase between 0 and $\boldsymbol{T}_r$. The phase is incremented by 1 unit at each iteration and when it reaches $\boldsymbol{T}_r$, the clock is reset to 0. The cell pauses to reverse its orientation, that is, we set

$$\boldsymbol{V}_k(t + \Delta t) = \boldsymbol{0},\ \boldsymbol{C}_k(t + \Delta t) = -\boldsymbol{C}_k(t), \tag{3}$$

where $\boldsymbol{C}_k(t)$ is the orientation of cell k at time t given by (1).

International Journal of Mathematical Modeling and Applied Computing
Vol. 1, No. 6, September 2013, PP: 26-40
Available online at http://acascipub.com/Journals.php

A-motility

In modeling the A-motility, we take into consideration both the effect of EPS slime secretion from the lagging pole of the cell and the cell's ability and tendency to follow the slime trail previously deposited by other cells. The cell orientation comes into play as the slime secretion from the rear end of the cell pushes the cell directly forward (Wolgemuth et al, 2002). We model this motility by trying to orient the cell along its long axis, which is given by the normalized cell orientation (1).

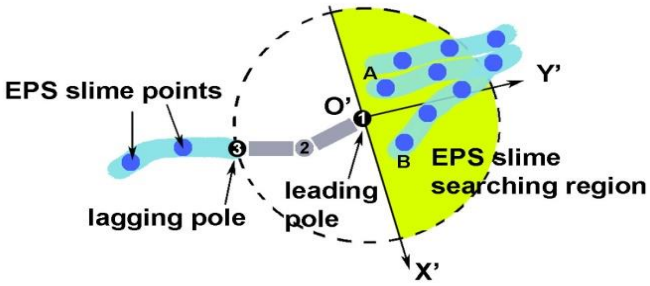

Figure 2: An illustration for the A-motility. A cell deposits EPS slime from its lagging pole (node 3) as it moves while searching for existing EPS slime in the vicinity of its leading pole (node 1).

As a cell moves forward, it leaves behind trails of EPS slime. In our discrete model, we keep track of the cell position by keeping track of the position of each node. Likewise, we keep track of the slime trail by keeping track of the position of the slime points. When a moving cell encounters a slime trail (or slime point), it tends to turn to an acute angle to follow the trail. To model this behavior, we first define the *EPS slime searching region* to be the semi-circular region around the leading pole with radius equal to the cell length (see Figure 2). If there are more than one slime points within the slime searching circle that satisfy the acute angle requirement, then the cell moves toward the region that contains more EPS points, which in the experiments corresponds to higher EPS concentration. Figure 2 illustrates a motile cell that deposits EPS slime points from its lagging pole while at the same time senses EPS slime from its leading pole. The slime searching region is colored in yellow. Here, the cell turns in the direction towards the slime point *A* instead of *B* since the sub-region in which *A* lies contains 5 slime points while the sub-region that contains *B* only has 2 slime points. The direction driven by slime following ability is given by

$$\boldsymbol{L}_k = \frac{\boldsymbol{s}_A - \boldsymbol{n}_k^1}{\|\boldsymbol{s}_A - \boldsymbol{n}_k^1\|}, \text{ such that } \boldsymbol{C}_k \cdot \boldsymbol{L}_k \geq 0 \qquad (4)$$

where $\boldsymbol{s}_A$ is the vector position of the slime point *A*. Note that the inequality in (4) is needed to ensure that when a cell turns toward a slime point, it makes an acute angle relative to its orientation. This avoids the possibility that a cell bends too much, which is not physically reasonable.

Let $\alpha_k(t)$ and $\beta_k(t)$ denote the weights of $\boldsymbol{C}_k(t)$ and $\boldsymbol{L}_k(t)$, respectively, at time *t*. Since the cell has the tendency to follow the slime trails, the algorithm first searches for the slime points nearby. If it finds at least one slime point within its searching circle that satisfies the acute angle requirement, then we set $\beta_k(t) = 1$. Otherwise $\beta_k(t) = 0$, which corresponds to the situation where there is no slime trail found inside the slime searching circle. In this case, the cell moves according to its orientation with some small random turning angle $\hat{\theta}$. This is based on experimental observation that cells may actively bend and turn even though there is no slime trail nearby (Hendrata et al, 2011). The formula for the A-motility direction is then given by

International Journal of Mathematical Modeling and Applied Computing
Vol. 1, No. 6, September 2013, PP: 26-40
Available online at http://acascipub.com/Journals.php

$$\boldsymbol{A}_k(t+\Delta t) = \alpha_k(t)[\boldsymbol{C}_k(t) + \vec{\epsilon}\, dB_k(t)] + \beta_k(t)\boldsymbol{L}_k(t) \quad (5)$$

with

$$\alpha_k(t) = \begin{cases} 1 & \text{if } \beta_k(t) = 0 \\ 0 & \text{if } \beta_k(t) = 1 \end{cases} \text{ and } \vec{\epsilon}\, dB_k(t) = \left(\cos\hat{\theta}, \sin\hat{\theta}\right).$$

From laboratory observation, it is known that the random turning angle $\hat{\theta}$ follows a random normal distribution with mean 30°, standard deviation 5° and maximum 60° (Hendrata et al, 2011).

S-motility

The social interaction arise in S-motility is mediated by type IV pili that extend from the cell's frontal pole and whose average length is approximately equal to one cell length. Once a cell anchors its pili to a neighboring cell, the pili then retract and pull the cell body forward.

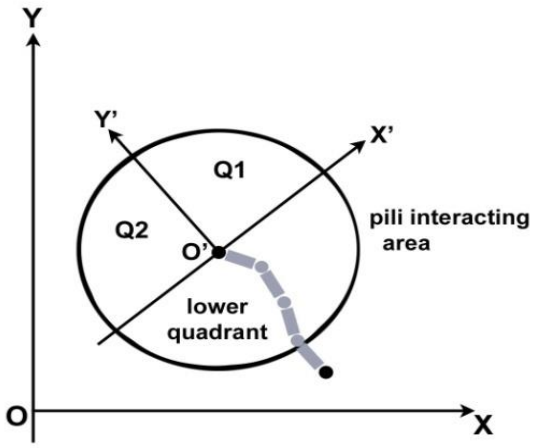

Figure 3: Pili interacting area in S-motility algorithm. The pili interacting area represents the vicinity of the pili and its radius can reach up to one cell length.

Similar to A-motility, we first define the *pili interacting area* to be the circular region centered at the head node whose radius is equal to a pilus length (see Figure 3). For algorithm implementation purposes, this region is divided into subregions Q1, Q2 and the lower quadrant, relative to the cell's local coordinate system X'O'Y' as shown in Figure 3. Each neighboring cell that lies inside this pili interacting area belongs to one of these subregions. By taking into consideration the same observation that a cell can only bend or turn to less than 90 degrees angle, we only allow the cell to move to either Q1 or Q2. Thus, if either Q1 or Q2 is not empty, then the cell moves towards the region whichever one that has the greatest number of distinct cells. The orientations of the neighboring cells in this particular subregion are then averaged to get the S-motility direction of cell *k*:

$$\boldsymbol{S}_k = \begin{bmatrix}\cos\alpha \\ \sin\alpha\end{bmatrix}, \ \alpha = \frac{1}{N}\sum_{j=1}^{N} \emptyset_j, \quad (6)$$

where N is the number of distinct cells in the quadrant to which cell k is moving and $\emptyset_j$ is the position angle of cell j in this quadrant with respect to positive X'-axis.

Collision-resolving algorithm

Collision occurs whenever the leading pole of a cell collides with a node of another cell, that is, when the distance between them is less than one cell width. There are two possible cases:

1. *Pole-to-pole collision* occurs when the leading pole of cell *k* collides with the leading pole of cell *j*. This type of collision is resolved by allowing cell *k* to randomly chooses, with uniform probability, to either reverses its orientation (3), or slightly changes its orientation by some small random angle away from cell *j*. The latter one is done by setting

$$\boldsymbol{V}_k(t+\Delta t) = R\boldsymbol{C}_k(t), \text{ where } R = \begin{bmatrix} \cos\delta & -\sin\delta \\ \sin\delta & \cos\delta \end{bmatrix}, \tag{7}$$

   is the rotation matrix with random angle $\delta \in [-5°, 5°]$.

2. *Pole-to-side collision* occurs when the leading pole of cell *k* collides with one of the non-leading nodes of cell *j*. Cell *k* then aligns to the acute angle with cell *j*. That is,

$$\boldsymbol{V}_k(t+\Delta t) = \operatorname{sgn}\big(\boldsymbol{C}_k(t)\cdot\boldsymbol{C}_j(t)\big)\,\boldsymbol{C}_j(t). \tag{8}$$

The direction vector $\boldsymbol{V}_k(t)$ of cell *k* in equation (2) is then determined by checking in the following order:

1. Checking the reversal clock to determine if cell *k* needs to reverse. If it does, we apply equation (3). Else, go to step 2.
2. Checking for any collision and follow collision-resolving algorithm if it occurs. Otherwise, go to step 3.
3. Define $\boldsymbol{V}_k$ to be a weighted unit direction due to A and S-motility, that is,

$$\boldsymbol{V}_k(t+\Delta t) = \frac{\gamma_k\boldsymbol{A}_k(t+\Delta t) + \delta_k\boldsymbol{S}_k(t+\Delta t)}{\|\gamma_k\boldsymbol{A}_k(t+\Delta t) + \delta_k\boldsymbol{S}_k(t+\Delta t)\|} \tag{9}$$

   where γ_k and δ_k are the weights of A and S-motility terms (equations (5) and (6)) of cell *k*, respectively. The motility weights for A-S+ mutants are taken to be $\gamma_k = 0$ and $\delta_k = 1$ and vice versa for the A+S- mutants. The wildtype A+S+ cells have both A and S-motility engines and we assign the weights randomly such that

$$\gamma_k \epsilon \{0,1\}, \qquad \delta_k = 1 - \gamma_k$$

   at any particular time *t*.

Scaling Laws

One challenge in simulating a biological system is that there are too many particles or cells to simulate. In a typical swarming colony of myxobacteria, one can expect to have more than 10^7 cells. It is very computationally expensive, if not impossible, to simulate all of them. One remedy is to simulate a much smaller number of cells and treat each cell in the simulation as a *superindividual*. Each superindividual represents a certain number of cells in the actual experiment, all of which behave in an identical manner as a single individual. The scaling law we derive in this section justifies that the dynamics of a colony of superindividuals in the simulation is identical to the dynamics of the actual biological colony. The colony behavior and the spatial patterns it exhibits need to be preserved, and moreover, the emergence of macroscopic system behavior needs to occur at the correct timing regardless of the number of cells in the simulation. The scaling law also determines how the parameters in the model are related to one another.

From (2), we deduce the relationship

$$\Delta x = v\,\Delta t \tag{10}$$

where Δx is the distance a cell travels during the time interval Δt. Here Δx and Δt are used as a measure of the spatial and temporal resolutions, respectively. The cell velocity v is kept constant in the simulation. Two other parameters r_p and r_s, which correspond to the radii of pili interacting area and slime searching region, respectively, need to be considered since they are linearly proportional to the cell length and they affect the behavior of the system. Thus, from (10), the linear scaling relationship between various parameters is given by: $\Delta t \propto \Delta x \propto r_p \propto r_s$.

Changing the number of particles (superindividuals) in the system requires the values of other parameters to be scaled by a scaling factor, say α, in order to keep the dynamics of the simulations comparable. To do this, let us first consider a simulation domain of area A, which we divide into small squares, each of which has sides that are equal to Δx. Let N be the number of cells in an actual laboratory experiment and n be the number of superindividual cells in a square. We keep n constant to ensure the consistency in the dynamics of the simulations. The density of this computational square is given by $\rho = n/\Delta x^2$. Assuming the density is uniform throughout the entire domain, the total number of superindividuals in our simulation is $n_T = nA/\Delta x^2$ and the number of cells each superindividual represents is given by

$$\beta = \frac{N}{n_T} = \frac{N\,\Delta x^2}{n\,A}. \tag{11}$$

Ideally, to capture the cell's individual behavior and its interaction with other cells, one would like to have $\beta = 1$. In other words, one cell in the simulation represents one cell, instead of a group of cells, in the actual experiment. Hence, it is desirable to keep β as small as possible and consider how β scales in relation to Δx. From (11), we obtain the relationship

$$n = \frac{N\,\Delta x^2}{\beta\,A}. \tag{12}$$

We would like to keep n constant regardless of the spatial resolution. To understand why this is a natural requirement, it is best to think about the increased computational resolution graphically as zooming in the field of view. As we zoom in on the smaller computational square, we increase the number of particles so that the number of particle in each new computational square is a constant n. The ultimate desirable computational square is so small that the number of particles in it is biologically correct, that is, each superindividual would represent a single cell. Here, N and A are also fixed. Let Δx_0 and β_0 respectively denote the spatial resolution and the number of cells represented by a superindividual in a reference simulation that gives us the behavior or pattern as observed in experiment. Since n is constant, equation (12) gives us the relationship

$$\frac{N\,\Delta x^2}{\beta A} = \frac{N\,\Delta x_0^2}{\beta_0\,A} \Rightarrow \Delta x = \sqrt{\frac{\beta}{\beta_0}}\,\Delta x_0.$$

Thus, the scaling factor is given by $\alpha = \sqrt{\beta/\beta_0}$.

International Journal of Mathematical Modeling and Applied Computing
Vol. 1, No. 6, September 2013, PP: 26-40
Available online at http://acascipub.com/Journals.php

Results and Discussion

Pattern comparison in large simulations

Before running large simulations, it is desirable to test and justify the motility algorithms described in Materials and Method (Mathematical Model). For this purpose, we simulate each A+S-, A-S+ and A+S+ cells at the edge of a swarming colony.

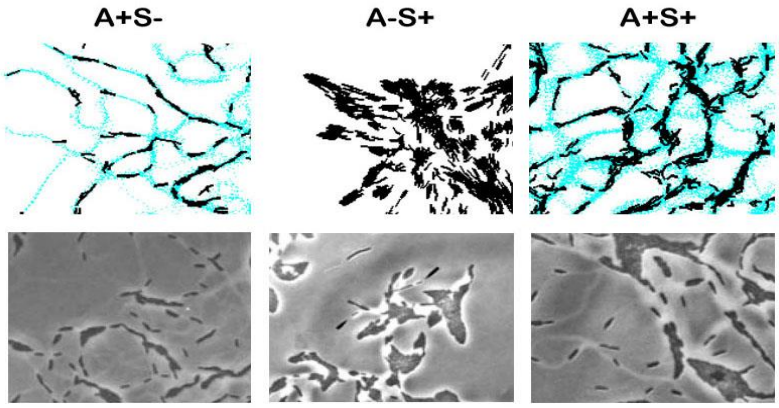

Figure 4: Comparison of the simulation with the experiment during the initial swarming stage. The bottom row shows the experimental results for each mutant (Wolgemuth et al, 2002), and the top row shows simulation results based on the discrete model described in Materials and Method (Mathematical Model). The slime trails produced and left by A+S- and A+S+ cells are also shown (colored in blue).

From Figure 4 we see that different mutants exhibit different behavior and different clustering patterns depending on their motility engine(s) that facilitates their interactions. The first column shows A+S- cells whose one prominent characteristic is that they move freely by themselves following the slime trails, and hardly form groups (Pelling et al, 2006). Therefore, even though several cells may come together, the clusters they form are long and stringy. In contrast, A-S+ cells prefer moving in groups (McBride, 2001). Their clusterings are shorter, thicker and shaped like arrowheads. The wildtype (A+S+) cells exhibit combined patterns of A-S+ and A+S- cells. They form thicker clumps than those of A+S-, and also longer than A-S+ clusters. Some cells can move individually, but they also have a tendency to group. These phenotypic agreements justify our algorithm and indicate a possible predictive potential of our model for the social behaviors of other uncharacterized myxobacteria mutants.

With the scaling law and the scaling factor α derived in Materials and Method (Scaling laws), we are interested in enhancing the computation by simulating more quantitatively accurate number of cells. With this, our goal is to simulate the cell motion deep inside a swarming colony with a much higher cell density.

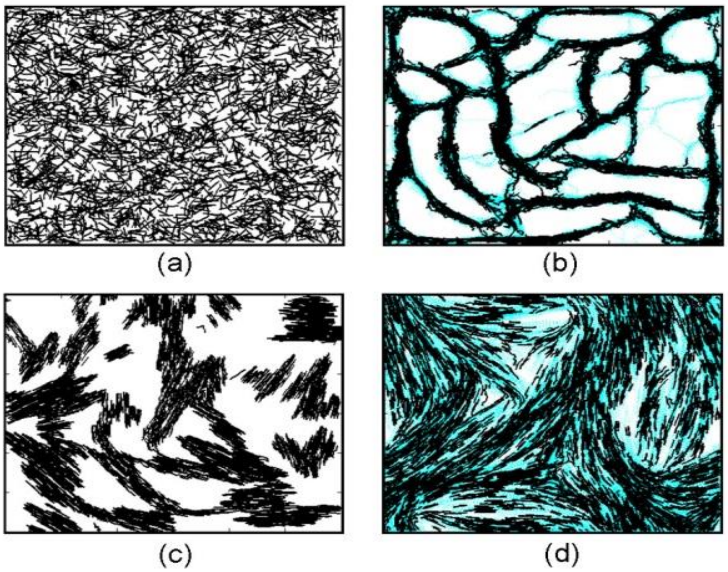

Figure 5: Reference simulation of 2880 superindividual cells inside a swarming colony. (a) Initial setup where cells are placed randomly in a square domain with periodic boundary condition. Distinct global patterns of (b) A+S-, (c) A-S+, and (d) A+S+ cells after 2 hours of evolution.

Klett-Summerson (K-S) unit is the unit of measurement of cell density in suspension (Kaiser, Crosby, 1983). A sample of cell suspension with 1 K-S unit has approximately 4×10^6 cells/ml. Using the experimental data, it is known that 100 K-S units correspond to a close-packing arrangement of cells in a two-dimensional area (Kaiser, Crosby, 1983; Wu et al, 2007). We choose cell density of 50 K-S unit (2×10^8 cells/ml) to give sufficient space between cells to use their A or S-motility and to interact with one another. Each petri dish (well) in an experiment contains approximately 15 μl of cell suspension. Thus, in 50 K-S density there are approximately 3×10^6 cells.

In our simulation setup, 50 K-S density unit is equivalent to having 2880 cells in $120\ \mu\text{m} \times 120\ \mu\text{m}$ square domain. These cells are superindividuals, each of which represents approximately 1041 biological cells. We place these cells randomly throughout the domain and use periodic boundary, which means that if a cell hits a boundary, then it will reappear at the opposite side of the boundary. The use of periodic boundary is appropriate to simulate a small part of a large system that is far from its edge. The global patterns for A+S-, A-S+ and A+S+ mutants after 2 hours of evolution are shown in Figure 5(b),(c),(d), respectively.

International Journal of Mathematical Modeling and Applied Computing
Vol. 1, No. 6, September 2013, PP: 26-40
Available online at http://acascipub.com/Journals.php

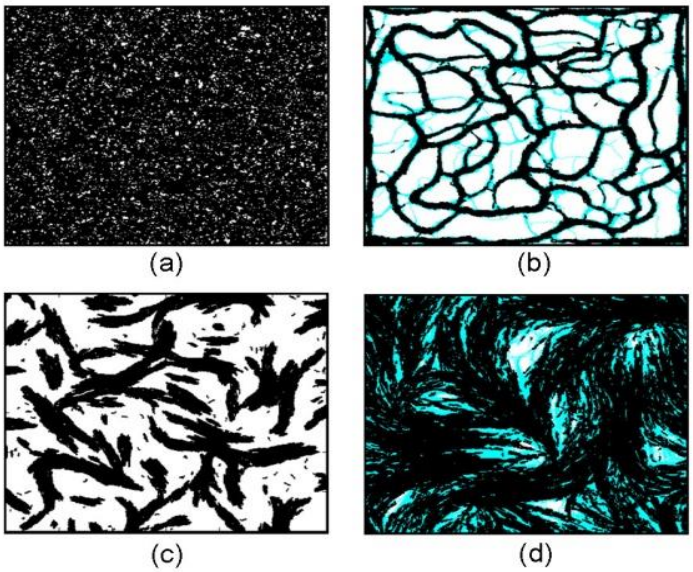

Figure 6: Scaled-up simulation of 20,000 superindividual cells inside a swarming colony. (a) Cells are placed randomly in a square domain with periodic boundary condition. Distinct global patterns of (b) A+S-, (c) A-S+, and (d) A+S+ cells are shown after 2 hours of evolution.

We can check the consistency of the patterns by simulating a larger number of cells. Having our codes implemented in faster platform, such as C++, we are able to scale up and simulate 20,000 superindividual cells. This is a significant improvement since now a superindividual in our simulation only represents 150 individual cells and this gives us the scaling factor $\alpha = \sqrt{\frac{150}{1041}} \approx 0.38$. We see that the similarities in the global patterns produced by the reference simulation with 2880 cells and simulation with 20,000 cells are prominent, as shown in Figure 6, indicating that these patterns are preserved regardless of the number of cells.

Order of collective motion

We now discuss the *order parameter* as a way to characterize collective motion of bacteria in swarms with complex clustering patterns. By computing the order parameter for each A+S-, A-S+ and A+S+ cells, we can quantify the global pattern for each of these mutants and suggest that the social interaction associated with the S-motility leads to an increase in the order parameter.

We adopt a version of the order parameter by Wu et al (2007), specifically designed for myxobacterial swarming. A state is called purely non-ordered when either all cells are isolated, or when there is a uniform distribution in the orientations of neighboring cells of any given cell. On the opposite side of the spectrum, a state is called most ordered when all cells are in direct contact with one another and move side by side in the same or opposite direction. Notice that we consider two opposite directions as being equivalent since myxobacteria cells reverse their polarity periodically. In addition, since cell-cell interactions often times cause the cells to cluster, we need to take into account the cell's alignment with its neighboring cells when measuring the global order of motion. Thus, the order contributed by a single cell is measured locally by considering both its position and its orientation.

International Journal of Mathematical Modeling and Applied Computing
Vol. 1, No. 6, September 2013, PP: 26-40
Available online at http://acascipub.com/Journals.php

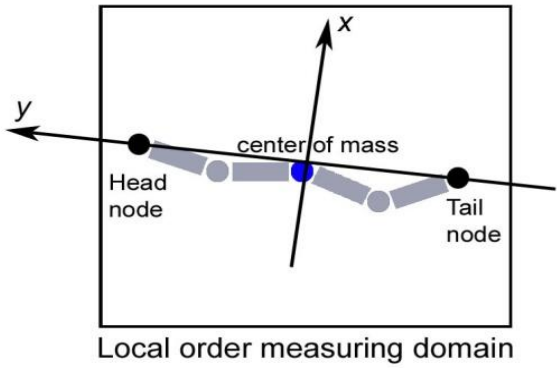

Figure 7: A cell with its local order measuring domain. Other cells which are located inside this rectangular domain are considered the neighbors of this cell.

We define the direct neighborhood of cell *k*, called the *local order measuring domain*, to be the rectangular region centered at the cell's center of mass whose length and width are equal to cell length, as shown in Figure 7. Any other cell *j* that lies inside this region is considered the neighbor of cell *k*. In computing the order parameter, there are two components to consider, namely the *local positional order P* and the *local orientational order* Ψ. We define the local positional order P_k of cell *k* as follows:

$$P_k = \begin{cases} N_k/N_0, & \text{if } N_k < (N_0/2) \\ 1, & \text{otherwise} \end{cases}. \tag{13}$$

Here N_k is the number of neighboring cells of cell *k* and N_0 is a predefined constant.

To compute the local orientational order, we first let $\boldsymbol{C}_k$ and $\boldsymbol{C}_j$ to be cell *k* and cell *j*'s orientations as defined by equation (1). We then take $\widetilde{\boldsymbol{C}_j} = \text{sgn}(\boldsymbol{C}_j \cdot \boldsymbol{C}_k)\boldsymbol{C}_j$. For each neighbouring cell $j = 1,2,\dots,n$, we compute $\theta_j \in [0,\pi]$, which is the angle between $\widetilde{\boldsymbol{C}_j}$ and the *x*-axis of cell *k*'s local coordinate system shown in Figure 7. The local orientational order Ψ_k is defined by

$$\Psi_k = \begin{cases} 0, & \text{if } n = 0 \text{ (cell } k \text{ has no neighbors)} \\ \frac{\Phi_k - \Phi_0}{1-\Phi_0}, & \text{otherwise} \end{cases} \tag{14}$$

where

$$\Phi_k = \frac{1}{(n-1)n} \sum_{\substack{l,m=1 \\ l \neq m}}^{n} \exp(-\left|e^{i2\theta_l} - e^{i2\theta_m}\right|) \tag{15}$$

and

$$\Phi_0 = \frac{1}{(n-1)n} \sum_{\substack{l,m=1 \\ l \neq m}}^{n} \exp(-\left|e^{i2\pi l/n} - e^{i2\pi m/n}\right|) \tag{16}$$

Note that Φ_k, which is scaled to have a range between 0 and 1, measures the distribution of θ_j. When all θ_j are equal, then $\Phi_k = 1$, which implies that $\Psi_k = 1$ and this corresponds to the most ordered state. For the case of uniform random distribution of θ_j, then $\Psi_k = 0$.

Combining both local positional and local orientational orders, the global order parameter for the collective motion is defined to be

$$\Omega = \frac{1}{M}\sum_{k=1}^{M} \Psi_k \cdot P_k, \tag{17}$$

where *M* is the total number of cells.

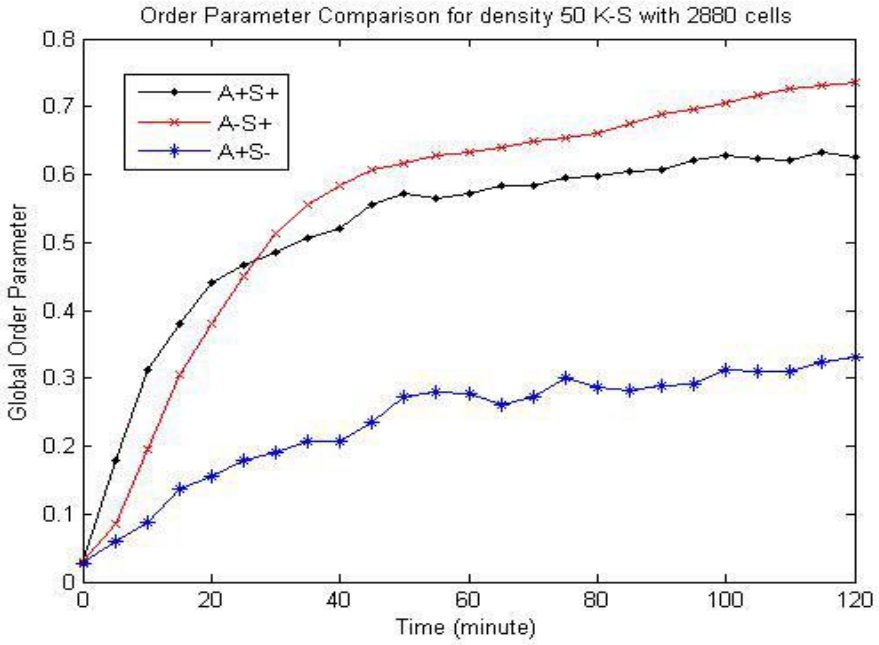

Figure 8: Plot of the order parameter Ω versus time for the simulations of A-S+, A+S- and A+S+ cells in 50 K-S density unit with 2880 (superindividual) cells (Figure 5). The order parameter of A-S+ is the highest at the end of 2 hours of evolution, while the A+S- has the lowest order. This indicates the role of social motility in cell-cell alignment.

We analyze and compare the local order parameter for each myxobacteria mutant in Figure 5 and 6. The order parameter Ω is computed for every 5 minutes of evolution up to 2 hours. Plot of the order parameters versus time of the reference simulation with 2880 superindividuals and the scaled up simulation with 20,000 superindividuals are shown in Figures 8 and 9, respectively.

From Figure 8, one can see that the order parameter of A+S- mutant increases linearly, while the order parameters of A-S+ and A+S+ mutants increase exponentially and they achieve a much higher order than A+S-. This tells us that the S-motility driven by pili facilitates cell-cell alignment and leads to the increase in the order parameter. On the other hand, the existence of A-motility enables the cells to move individually, and as a consequence, large multicellular domains in which cells are found aligned and in contact are hardly present. This finding is very similar

to the one by Pelling at al (2006) in which they used the atomic force microscope to apply the angular domain mapping analysis of domain formation of different mutants of myxobacteria. Another interesting point worth noticing is during the first 30 minutes, the order parameter of A+S+ cells is higher than A-S+, but from that point on the order of A-S+ picks up and becomes higher than A+S+. This indicates that during the initial swarming stage, cells require both A and S-motility systems to efficiently achieve high degree of self-organization and parallel alignment of cells. Lastly, based on the experimental observation that the wildtype A+S+ cells have the highest chance to develop fruiting bodies, thus leading to greater colony survival rates, it appears that there may be a trade-off between cell alignment and the ability to form the fruiting body effectively. As a future project, we plan to investigate a certain range in the degree of alignment measured by the order parameter that is most favorable for the development, and also for the entire life-cycle.

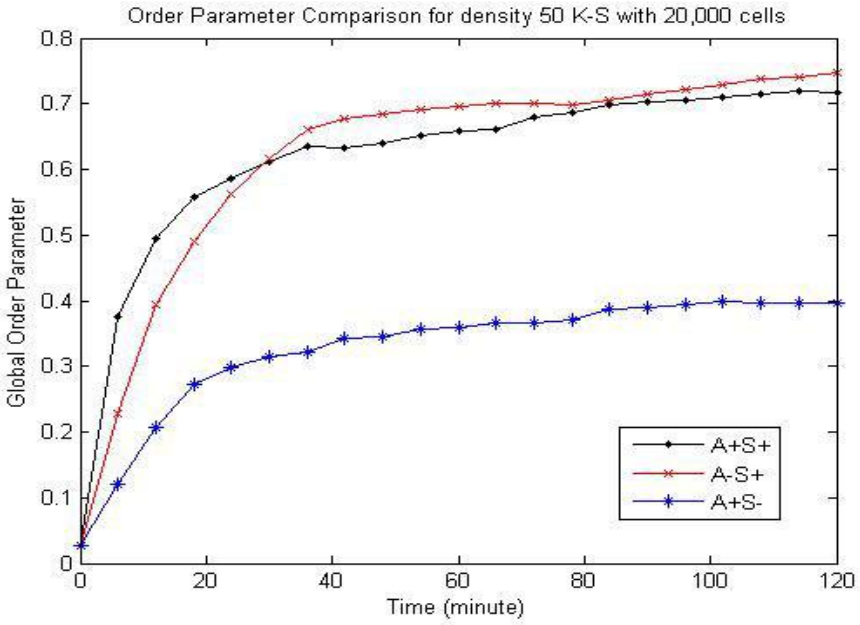

Figure 9: Order parameter comparison for A-S+, A+S- and A+S+ cells in 50 K-S density unit with 20,000 (superindividual) cells. The order parameter of A-S+ is the highest at the end of 2 hours of evolution. This trend is similar to Figure 8. In particular, note that the turning point at which the order of A-S+ becomes higher than A+S+ occurs at approximately 30 minutes, as shown previously in Figure 8.

Conclusion

We present an off-lattice cell-based model to simulate the swarming behavior of different mutants of myxobacteria. In a cell-based model, cell movement is governed entirely by motility algorithms, hence it offers transparency and flexibility. The concept of superindividual enhances the computation and allows us to simulate larger number of cells, and therefore it overcomes computational complexity and better demonstrates the global behavior of the system. The scaling law derived for the model justifies that the dynamics of the superindividuals is identical to those of the actual population. We obtain good phenotypic agreement of the swarming patterns produced by our simulation and those observed in experiments. This indicates the accuracy of the model and its potential to predict the social behavior of other unknown mutants. Furthermore, with our large scale simulation, we quantify different global swarming patterns for different myxobacteria mutants and show the significant role of social motility driven by pili in cell-cell alignment.

References

[1] Alber, M., Kiskowski, M., Jiang, Y., Two-stage aggregate formation via streams in myxobacteria, Phys. Rev. Lett., 93, 6, 2004, 068102.

[2] Blackhart, B., Zusman, D., Frizzy genes of myxococcus xanthus are involved in control of frequency of reversal of gliding motility, Proc. Natl. Acad. Sci USA, 82, 24, 1985, 8767-8770.

[3] Burchard, R. P., Trail following by gliding bacteria, J. Bacteriol., 152, 1, 1982, 495-501.

[4] Gallegos, A., Mazzag, B., Mogilner, A., Two continuum models for the spreading of myxobacteria swarms, Bull. Math. Biol., 68, 4, 2006, 837-861.

[5] Hendrata, M., Birnir, B., Dynamic-energy-budget-driven fruiting-body formation in myxobacteria, Phys. Rev. E, 81, 2010, 061902.

[6] Hendrata, M., Yang, Z., Lux, R., Shi, W., Experimentally guided computational model discovers important elements for social behavior in Myxobacteria, PLoS ONE, 6, 7, 2011, e22169.

[7] Hodgkin, J., Kaiser, D., Genetics of gliding motility in Myxococcus xanthus: genes controlling movement of single cells, Mol. Gen. Genet., 171, 2, 1979, 167-176.

[8] Holmes, A., Kalvala, S., Whitworth, D., Spatial simulations of myxobacterial development, PLoS Comput. Biol., 6, 2, 2010, e1000686.

[9] Igoshin, O., Kaiser, D., Oster, G., Breaking symmetry in myxobacteria, Curr. Biol., 14, 2004, R459-462.

[10] Kaiser, D., Coupling cell movement to multicellular development in myxobacteria, Nat. Rev. Microbiol., 1, 1, 2003, 45-54.

[11] Kaiser, D., Crosby, C., Cell movement and its coordination in swarms of Myxococcus xanthus, Cell Motility, 3, 3, 1983, 227-245.

[12] Kaiser, D., Yu, R., Reversing cell polarity: evidence and hypothesis, Curr. Opin. Microbiol., 8, 2, 2005, 216-221.

[13] Kiskowski, M., Jiang, Y., Alber, M., Role of streams in myxobacteria aggregate formation, Phys. Biol., 1, 3-4, 2004, 173-183.

[14] McBride, M., Bacterial gliding motility: multiple mechanisms for cell movement over surfaces, Annu. Rev. Microbiol., 55, 2001, 49-75.

[15] Pelling, A. E., Li, Y., Cross, S., Castaneda, S., Shi, W., Gimzewski, J. K., Self-organized and highly ordered domain structures within swarms of Myxococcus xanthus, Cell Motil. Cytoskeleton, 63, 3, 2006, 141-148.

[16] Shi, W., Yang, Z., Sun, H., Lancero, H., Tong, L., Phenotypic analyses of frz and dif double mutants of Myxococcus xanthus, FEMS Microbiol. Lett., 192, 2, 2000, 211-215.

[17] Sozinova, O., Jiang, Y., Kaiser, D., Alber, M., A three-dimensional model of myxobacterial aggregation by contact-mediated interactions, Proc. Natl. Acad. Sci USA, 102, 32, 2005, 11308-11312.

[18] Sozinova, O., Jiang, Y., Kaiser, D., Alber, M., A three-dimensional model of myxobacterial fruiting-body formation, Proc. Natl. Acad. Sci USA, 103, 46, 2006, 17255-17259.

[19] Wolgemuth, C., Hoiczyk, E., Kaiser, D., Oster, G., How myxobacteria glide, Curr. Biol., 12, 5, 2002, 369-377.

[20] Wu, Y., Chen, N., Rissler, M., Jiang, Y., Kaiser, D., Alber, M., CA Models of Myxobacteria Swarming, ACRI Springer-Verlag, LNCS 4173, 2006, 192-203.

[21] Wu, Y., Jiang, Y., Kaiser, D., Alber, M., Social interactions in myxobacterial swarming, PLoS Comput. Biol., 3, 12, 2007, e253.